

Facing the wind of the pre-FUor V1331 Cyg ^{*}

P.P. Petrov ^{1†}, R. Kurosawa², M.M. Romanova³, J.F. Gameiro⁴, M. Fernandez⁵,
E.V. Babina¹ and S.A. Artemenko¹

¹Crimean Astrophysical Observatory, Taras Shevchenko National University of Kiev, 98409 Nauchny, Crimea, Ukraine

²Max-Planck-Institut für Radioastronomie, Auf dem Hügel 69, 53121 Bonn, Germany

³Cornell University, 310 Space Sciences Building, Ithaca NY, 14853 USA

⁴Centro de Astrofísica e Faculdade de Ciências da Universidade do Porto, Rua das Estrelas, 4150-762 Porto, Portugal

⁵Instituto de Astrofísica de Andalucía, CSIC, Glorieta de la Astronomía, 3, E-18008 Granada, Spain

June 19, 2014

ABSTRACT

The mass outflows in T Tauri stars (TTS) are thought to be an effective mechanism to remove angular momentum during the pre-main-sequence contraction of a low-mass star. The most powerful winds are observed at the FUor stage of stellar evolution. V1331 Cyg has been considered as a TTS at the pre-FUor stage. We analyse high-resolution spectra of V1331 Cyg collected in 1998–2007 and 20-d series of spectra taken in 2012. For the first time the photospheric spectrum of the star is detected and stellar parameters are derived: spectral type G7–K0 IV, mass 2.8 M_⊙, radius 5 R_⊙, $v \sin i < 6 \text{ km s}^{-1}$. The photospheric spectrum is highly veiled, but the amount of veiling is not the same in different spectral lines, being lower in weak transitions and much higher in strong transitions. The Fe II 5018, Mg I 5183, K I 7699 and some other lines of metals are accompanied by a ‘shell’ absorption at radial velocity of about -240 km s^{-1} . We show that these absorptions form in the post-shock gas in the jet, i.e. the star is seen through its jet. The P Cyg profiles of H α and H β indicate the terminal wind velocity of about 500 km s^{-1} , which vary on time-scales from several days to years. A model of the stellar wind is developed to interpret the observations. The model is based on calculation of hydrogen spectral lines using the radiative transfer code TORUS. The observed H α and H β line profiles and their variability can be well reproduced with a stellar wind model, where the mass-loss rate and collimation (opening angle) of the wind are variable. The changes of the opening angle may be induced by small variability in magnetization of the inner disc wind. The mass-loss rate is found to vary within $(6–11) \times 10^{-8} \text{ M}_{\odot} \text{ yr}^{-1}$, with the accretion rate of $2.0 \times 10^{-6} \text{ M}_{\odot} \text{ yr}^{-1}$.

Key words: stars: individual: V1331 Cyg – stars: variables: T Tauri – stars: variables: Herbig Ae/Be – stars: winds, outflows.

1 INTRODUCTION

T Tauri stars (TTS) are pre-main-sequence (PMS) objects of low masses ($\leq 2 \text{ M}_{\odot}$) at ages of $\sim 1–10 \text{ Myr}$. The classical TTS (cTTS) still possess their accretion discs. The processes of mass accretion on to cTTS are responsible for the observed irregular light variability and the intensive emission

line spectra of the stars. The accretion is also thought to be the driving force of the observed mass outflows – winds and jets of cTTS. For review of the observational characteristics of cTTS and their models, see e.g. Bouvier et al. (2007) and Guenther (2013).

One of the intriguing problems of cTTS is the evolution of their angular momentum. In spite of high angular momentum of the accreting matter, most of cTTS rotate at less than 0.1 of their critical velocity, with periods of several days. There must be some mechanism to remove the excess of angular momentum from the star–disc system during the first million years of their evolution. The winds and jets formed in magnetohydrodynamic (MHD) processes are the probable agents through which cTTS lose their angular mo-

* Based on observations collected at the Keck Observatory, Hawaii, USA; the Centro Astronómico Hispano Alemán (CAHA) at Calar Alto, operated jointly by the Max-Planck Institut für Astronomie and the Instituto de Astrofísica de Andalucía (CSIC); the WHT telescope on La Palma, Spain; and the Crimean Astrophysical Observatory, Ukraine.
† E-mail: petrov@crao.crimea.ua; petrogen@rambler.ru

mentum. The large-scale open magnetic field connects the rotating star–disc system with the circumstellar medium, and the magnetized outflowing gas removes the mass and angular momentum from the system (Matt & Pudritz 2005).

Different configurations of the wind formation are possible, including a stellar wind similar to the solar one (Cranmer 2009), an X-wind, in which the outflow starts from the inner region of the disc (Shu et al. 1994), and a disc wind launched from the extended disc area (Pudritz et al. 2007). A conical wind model, launched from the inner disc and accelerated by magnetic pressure, was proposed by Romanova et al. (2009).

Observations may provide clues to the origin of outflows and constrain the models. Comparison of the observed diagnostic line profiles with those predicted by the models is a usual tool in the study of the accretion and outflow processes in cTTS (e.g. Edwards et al. 2006). Major recent efforts are from Kurosawa, Romanova & Harries (2011) and Kwan & Fischer (2011), who studied the effect of the winds on the formation of hydrogen and helium lines in optical and near-infrared, using their radiative transfer model.

The mass-loss rates in cTTS are typically within 10^{-9} – 10^{-7} M_{\odot} yr^{-1} . Extreme case of mass-loss can be seen in the FU Ori stars (FUors). This stage of the PMS evolution may be considered as a dramatic episode of intensified transfer of angular momentum. It is widely agreed that the FUor phenomenon is an event of greatly enhanced accretion, and the intensive outflow is a consequence of this (Hartmann & Kenyon 1996; Audard et al. 2014). However, in one of the classical FUor, V1057 Cyg, which was a cTTS before its brightening in 1971, an extremely powerful wind already was present in 1958, about 12 years *before* the outburst (Herbig 2009). This suggests that the FUor progenitors are cTTS with enhanced mass-loss.

Among the cTTS there is a small group of stars which possess unusually strong winds, similar to those in FUors, and may possibly be progenitors of FUors. Apart from the typical P Cyg profiles, an obvious indicator of their dense, high-velocity winds is the abnormal ratio of the H and K Ca II emission lines: while the K line of Ca II (3933 Å) is prominent in emission, the H line (3968 Å) is absent because it is suppressed by the P Cyg absorption component of He (3979 Å) (Herbig, Petrov & Duemmler 2003). In other words, the wind is optically thick even in higher Balmer lines. This effect was also seen in the spectrum of V1057 Cyg before it went to FUor stage.

Three such extreme-wind cTTS, that are also relatively bright ($V < 13^m$), can be identified in the northern sky: V1331 Cyg, AS 353 A and LkHa 321. The study of these stars may shed light on the nature of the transition between the cTTS and FUor phases of the PMS evolution.

In this paper we present results of our research of V1331 Cyg. The star was earlier considered as a candidate in pre-FUors (Welin 1976; Herbig 1989; McMuldroch, Sargent & Blake 1993). Besides the strong emission line spectrum and strong wind features, the star is surrounded by a ring-like reflection nebula of about 30 arcsec in diameter (Kuhi 1964; Mundt & Eisloffel 1998). Such nebulae are present in classical FUors, indicating the past events of extensive mass-loss (Goodrich 1987). From the images of V1331 Cyg obtained by the *Hubble Space Telescope*, Quanz, Apai & Henning (2007) revealed yet another ring-like nebula closer to the star. They

concluded that the star is seen pole-on, along the axis of a conical outflow. Radio emission of CO molecule in mm wavelengths showed more complicated structure: a massive ($\approx 0.5 M_{\odot}$) disc around the star, bipolar flows and an expanding ring of about 10^4 au (McMuldroch et al. 1993). It was concluded that the previous FUor event of V1331 Cyg was about 4000 years ago.

Interestingly, the photospheric spectrum of the star has not been detected so far, and the spectral type and luminosity have been estimated from its spectral energy distribution, interstellar extinction and distance. Earlier estimations were B0.5 (Cohen & Kuhi 1979), A8–F0 (Chavarría 1981), F0 (Mundt et al. 1981), G0 (Kolotilov 1983). Later investigation by Hamann & Persson (1992) gave spectral type G5 and stellar luminosity $L_{*} = 21 L_{\odot}$, with distance $d = 700$ pc and extinction $A_v = 1.4^m$. The low dispersion IUE spectrogram at $\lambda 2200$ – 3200 Å is dominated by the Mg II resonance doublet emission (Mundt et al. 1981). No Balmer jump in emission is in the blue part of the spectrum (Valenti, Basri & Johns 1993). The visible region shows low excitation emission line spectrum of metals and the P Cyg features of Balmer lines of hydrogen. With near-IR interferometry, the dusty disc inner radius (at the distance of dust sublimation) was measured as 0.31 au (Eisner et al. 2007). V1331 Cyg is photometrically variable within $V=11.8$ – 12.4 (Kolotilov 1983; Fernandez & Eiroa 1996; Shevchenko et al. 2003). No rotational period was found from the available photometric data.

The aim of our research is to find an adequate model of wind of V1331 Cyg, which can describe the observed Balmer line profiles and their variability. We use high-resolution, high quality echelle spectra of V1331 Cyg, obtained in 1998, 2004 and 2007, and a series of spectra obtained in 2012 August.

2 OBSERVATIONS

One spectrum of V1331 Cyg was obtained at the 4.2m *William Herschel Telescope* of the Isaac Newton Group, using the Utrecht Echelle Spectrograph (UES), equipped with an echelle grating of 31 lines per mm and installed on the Nasmyth focus. The instrument yielded 67 orders spanning a wavelength range of ≈ 4650 – 10100 Å. A SITE2 chip 2048×2048 pixel CCD detector with $24 \mu\text{m}$ pixel was used. The spectral resolution $R \approx 50000$ and the signal-to-noise ratio (S/N) is about 150 at 6500 Å.

Two spectra of V1331 Cyg were obtained by George Herbig with the HIRES echelle spectrograph at Keck-1¹ on 2004 July 24 and 2007 November 23. In 2004, the CCD detector covered wavelength range of 4350–6750 Å. In 2007, a mosaic of three CCDs was used to cover the range of 4750–8690 Å. The data have the spectral resolution $R \approx 48000$, and the S/N=150–250.

In 2012, we carried out spectroscopic monitoring of

¹ The W. M. Keck Observatory is operated as a scientific partnership among the California Institute of Technology, the University of California, and the National Aeronautics and Space Administration. The Observatory was made possible by the generous financial support of the W. M. Keck Foundation.

Table 1. Log of observations

Site	Year	Date	Mid exposure HJD 245...		
La Palma	1998	Nov 7	1125.331		
Mauna Kea	2004	Jul 24	3210.553		
Mauna Kea	2007	Nov 23	4427.726		
Calar Alto	2012	Jul 28	6136.655		
		Aug 13	6152.518		
		Aug 14	6153.548		
		Aug 15	6154.640		
		Aug 16	6155.525		
		Aug 17	6156.677		
		Aug 18	6157.675		
		Aug 19	6158.653		
		Aug 20	6159.681		
		Aug 21	6160.676		
		Aug 22	6161.680		
		Crimea	2012	Aug 21	6161.277
				Aug 22	6162.407
Aug 23	6163.268				
Aug 24	6164.410				
Aug 25	6165.249				
Aug 26	6166.413				
Aug 27	6167.237				
Aug 30	6170.445				
Aug 31	6171.253				

V1331 Cyg during about 20 d with the aim to detect possible rotational modulation in emission line profile, which could help us to estimate the period of stellar rotation and characteristic time of the wind profiles variability. The observations were carried out in two observing sites: Calar Alto Observatory (Spain) and Crimean Astrophysical Observatory (Ukraine). The log of observations is given in Table 1.

Eleven spectra were obtained from July 28 to August 22, with the Calar Alto Fibre-fed Echelle (CAFE) attached to the Cassegrain focus of the 2.2m Telescope of the Calar Alto Observatory (CAHA). CAFE is a single-fibre, high-resolution ($R \approx 60000$) spectrograph, covering the wavelength range of 3650–9800 Å with 84 orders (Aceituno et al. 2013). The detector is an iKon-L camera with 2048x2048 pixels of 13.5 μm. In this set of spectra the S/N varies from night to night and its value for the continuum near the H α line is between 20 and 35.

Observations at Calar Alto were immediately followed by the run of the Crimean observations with the coude spectrograph of the 2.6-m Shajn reflector. Six consequent 30-min exposures were taken each night. The S/N in the Crimean spectra was lower than that in the Calar Alto spectra, and only H α region (6530–6600 Å) was covered. In order to increase the S/N, the Crimean spectra were smoothed by Gaussian filter with full width at half-maximum (FWHM) = 0.3 Å (13.7 km s⁻¹).

All the spectra were reduced in a standard way using the IRAF routines and normalized to continuum level. The spectral monitoring in 2012 was supported by UBV r photometry at the Crimean Astrophysical Observatory.

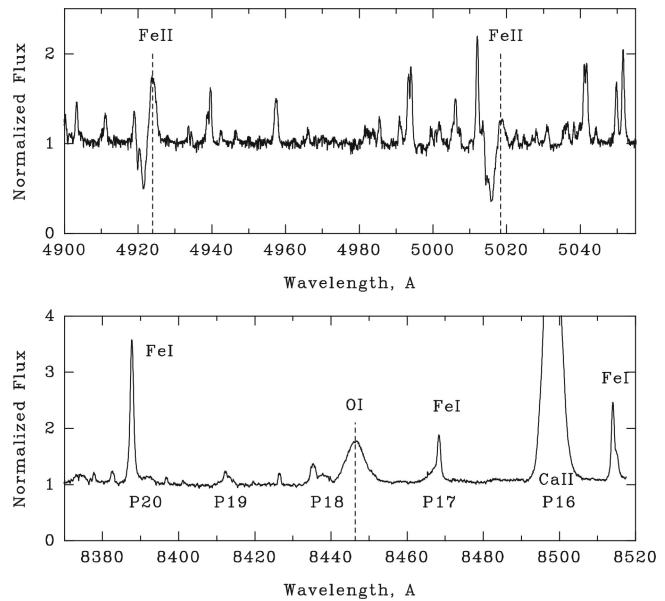


Figure 1. Two fragments of spectrum of V1331 Cyg in 2007. Wavelength scale is astrocentric. The vertical dashed lines mark laboratory wavelengths of the Fe II and O I lines.

3 RESULTS

Two fragments of spectrum of V1331 Cyg are shown in Fig 1. In this and the following figures, the wavelength scale is astrocentric. As in many other cTTS (e.g. Hamann & Persson 1992), the spectrum of V1331 Cyg consists of several components:

- 1) narrow veiled photospheric absorptions of a late-type star;
- 2) narrow emission lines of metals – neutrals and ions;
- 3) lines of Balmer and Paschen series, with P Cyg profiles;
- 4) narrow deep absorptions, blue-shifted by 150–250 km s⁻¹, in lines of Fe II, Mg I, Na I and others;
- 5) forbidden emission lines of [O I] and [S II].

In the following we consider in details each of these components.

3.1 Photospheric spectrum and stellar parameters

The photospheric spectrum of the star is best visible in the Keck spectra (Fig. 2), although the lines are very weak and narrow. In spite of the high resolution (6 km s⁻¹), the photospheric lines are not resolved: their width is the same as that of the weak telluric water lines. Thus, we may set only the upper limit for the projected rotational velocity of the star: $v \sin i < 6$ km s⁻¹. This is in agreement with the earlier conclusion that the star is seen pole-on. The radial velocity (RV) of the star $RV = -15.0 \pm 0.3$ km s⁻¹, with no difference between the spectra of 2004 and 2007.

The spectral classification of the highly veiled spectrum of cTTS is not a trivial task. The line ratios may be distorted by the chromospheric emission filling in the stronger lines, therefore the temperature and gravity criteria must be found among the weakest lines. We compared the photospheric spectrum of V1331 Cyg with a number of spectra

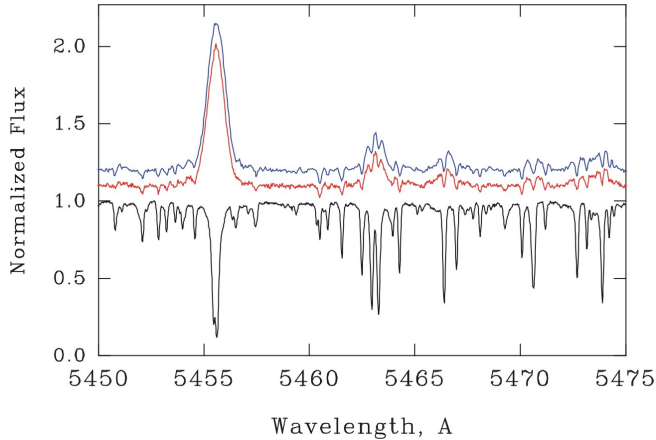


Figure 2. An example of the weak photospheric lines in V1331 Cyg, 2004 and 2007 (two upper curves). A template G7 IV spectrum is shown for comparison (lower curve).

downloaded from the VLT/UVES library², within spectral types G5–K2 and luminosities II–IV. Also available was the spectrum of β Aqr (G0 Ib–II), taken with the HIRES spectrograph at Keck-1. In addition, we used a grid of synthetic spectra in selected wavelength windows in order to find luminosity criteria. The spectra were calculated using the code by Berdyugina (1991) and Kurucz models. Atomic line data were retrieved from the VALD data base (Kupka et al. 2000). More detailed description of the spectral type and luminosity determination is given in a separate paper (Petrov & Babina 2014). As a result, the spectral type was found to be within G7–K0 IV, which corresponds to $T_{\text{eff}} = 5000\text{--}5250$ K, $\log g \approx 3.5$. This value of gravity indicates that the observed photospheric spectrum of V1331 Cyg is formed not in the disc atmosphere, as it could be in case of a FUor, but in the atmosphere of the star. With this temperature, assuming stellar luminosity $21 L_{\odot}$ (Hamann & Persson, 1992) the mass and radius of the star were derived using the grid of models by Siess, Dufour & Forestini (2000): $M_{*} \approx 2.8 M_{\odot}$, $R_{*} \approx 5 R_{\odot}$.

3.2 The peculiar veiling effect

The veiling of the photospheric spectrum in cTTS is usually attributed to the presence of an additional (non-photospheric) continuum, radiated by a hotspot on stellar surface. Then, the veiling factor (VF) = $\text{EW}(\text{std})/\text{EW}(\text{tts}) - 1$, where $\text{EW}(\text{tts})$ is equivalent width of a line in spectrum of TTS, and $\text{EW}(\text{std})$ is that in a standard star of the same spectral type. The VF is typically wavelength dependent, rising towards the blue part of the spectrum. In this interpretation, all the photospheric lines within a narrow spectral range must be reduced in EW by the same factor. However, detailed analysis of highly veiled cTTS spectra revealed that stronger lines are more affected by veiling than weaker lines, even those close in wavelength (Gahm et al. 2008, 2013; Petrov et al. 2011). It was interpreted as an effect of chromospheric emission

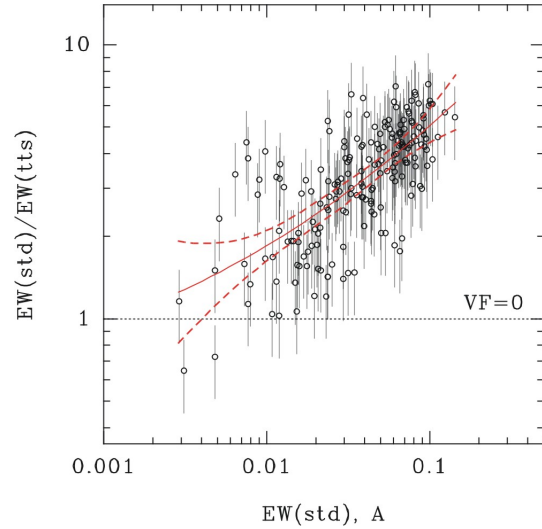


Figure 3. Ratio of equivalent widths in spectra of template (G7 IV) and V1331 Cyg is rising towards stronger lines. The line of regression and the 99 per cent confidence interval are indicated. The horizontal dotted line marks zero level of veiling.

filling in stronger lines, and was reproduced in a model of atmosphere heated by accretion (Dodin & Lamzin 2012).

This effect of the ‘chromospheric veiling’ is well expressed in V1331 Cyg. We measured equivalent widths of about 200 photospheric lines in V1331 Cyg and in the template stars. Fig. 3 shows the ratio of EWs as a function of EW in the template star. Stronger lines, with $\text{EW} = 50\text{--}100$ mÅ in the template spectrum, are reduced by a factor of ≈ 4 in V1331 Cyg, while the weaker lines are almost the same. The errors of EW measurements in V1331 Cyg are large, because the measured lines are very weak, from a few mÅ to about 20 mÅ. In the weakest lines ($\text{EW} < 5$ mÅ), the error is 30–50 per cent, for stronger lines it is about 20–30 per cent and caused mainly by the continuum level uncertainty.

The dependence shown in Fig. 3 still remains if another star, K1 IV, is used as a template spectrum. There was no sense to use earlier G-type templates, because the VF would become negative in weaker lines. Later K-type templates are also not adequate, because already in K3 star numerous metal lines of low ionization appear, which are certainly not present in V1331 Cyg. Another complication is the presence of the emission lines of metals: in stronger lines the photospheric absorption appears only as a dip on top of the broader emission (see Fig. 2). These lines were not included into analysis of EWs.

Hence, the VF, caused by a non-photospheric continuum in V1331 Cyg, as derived from the weaker photospheric lines ($\text{EW} < 10$ mÅ in the template star), is not well defined, but certainly does not exceed $\text{VF} = 1$. With this reservation, we do not find dependence of VF on either wavelength (from 4500 to 8500 Å) or excitation potential (EP) (from 0 to 6 eV) of the transitions.

3.3 Emission line spectrum

The emission line spectrum of V1331 Cyg is very rich in strong narrow ($\text{FWHM} = 40\text{--}60$ km s^{−1}) lines of neutral and ionized metals, rested at stellar RV. Intensities of the narrow

² <http://www.eso.org/sci/observing/tools/uvespop/>

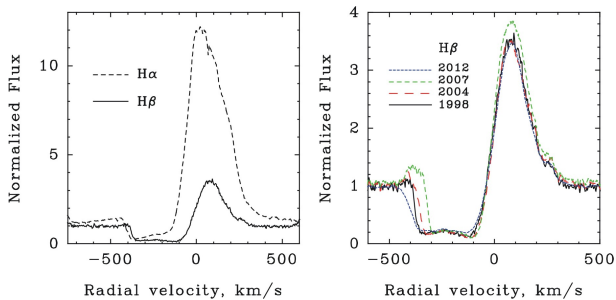


Figure 4. Balmer line profiles. Left: $H\alpha$ and $H\beta$ lines in 2007. Right: $H\beta$ line in different years of observations.

emission lines are similar in all the spectra of 1998–2012. The narrow emission lines in spectra of cTTS are usually attributed to chromospheric-like regions of post-shocked gas at the footpoints of accretion columns (Batalha et al. 1996; Beristain, Edwards & Kwan 1998). In the Keck spectra of V1331 Cyg, we measured EWs of 32 less blended emission lines of Fe I with EP of lower level from 0.9 to 4.5 eV, and EWs of seven lines of Fe II with EP from 2.9 to 3.9 eV. The curve of growth of these emission lines (Herbig 1990) gives $T_{\text{exc}} = 3800 \pm 300$ K and $\log N_e = 8 \pm 0.5$. This low electron density implies that the origin of the narrow emission lines in V1331 Cyg may be different from those in cTTS. The constancy of the emission lines also suggests their origin in a large volume of gas.

The broad emission lines are seen in the Balmer and Paschen series of hydrogen and the infrared Ca II triplet. Also broad lines, centred at stellar velocity, are those of high EP, e.g. He I 5876 Å (EP = 23 eV, FWHM ≈ 130 km s⁻¹) and O I 8446 Å (EP = 9.5 eV, FWHM ≈ 200 km s⁻¹). The He I 5876 emission is relatively weak, EW = 0.2 Å. The He II 4686 line is absent. In our spectra of V1331 Cyg, the observed ratio Ca II 8498 : O I 8446 = 6.5 ± 1.0 corresponds to $T_e \approx 8000$ K and $\log N_H \approx 10^{12}$ cm⁻³ (Kwan & Fischer 2011). Most likely, the lines are formed in stellar magnetosphere.

The forbidden emission lines of [O I] 6300 and 6363 Å, and [S II] 6716 and 6730 Å have strong peaks at RV of -240 km s⁻¹. The peak position remained the same in all the years of observations, while the overall profile changed from year to year. These lines represent low density gas, 10^4 to 10^6 cm⁻³ (e.g. Hartigan, Edwards & Ghandour 1995).

3.4 Wind features

The Balmer lines of H I show a classical P Cyg type profile, thus indicating a powerful mass outflow (Fig. 4). This characteristic is rare in cTTS but typical for FUors. In our spectra of V1331 Cyg, the $H\alpha$ and $H\beta$ profiles are slightly variable on a time-scale of days, while the spectra of different years show more significant differences. The terminal RV of the outflow varies between -350 and -450 km s⁻¹. The strong P Cyg absorption is also present in the resonance Na I D lines.

The characteristic pattern of variability is shown for $H\beta$ line on the right panel of Fig. 4, where profiles of 1998, 2004, 2007 and 2012 are overplotted. The spectrum of 2012 is an average of 10 nights of Calar Alto observations. The

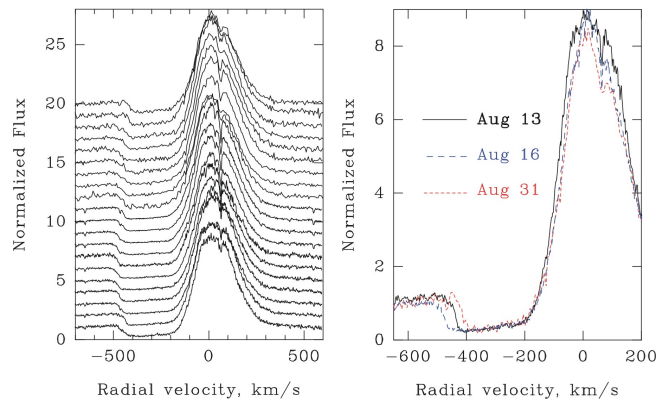


Figure 5. Monitoring of $H\alpha$ line in 2012. Left panel: night-to-night series, starting from July 28 (lower spectrum). Right panel: three spectra of 2012 August, showing typical variability in the wind terminal velocity.

variable is mostly the terminal velocity of the wind, while the emission peak remains about the same.

Fig. 5 shows a series of $H\alpha$ profiles in 2012 August, starting in Calar Alto and continued in Crimea. The same kind of variability can be seen in this 20-d series: terminal velocity of the outflow changes by 60 km s⁻¹ on a time interval of a few days. This is shown with the three overplotted profiles on the right panel of Fig 5. No periodic variations, presumably related to stellar rotation, were found in this 20-d monitoring. Analysis of the Balmer line profiles is given in Section 4.

During the spectral monitoring in 2012 the brightness of the star varied slightly within $V = 11.85$ – 12.08 , $B-V = 1.08$ – 1.16 . No correlation with any spectral parameter was found.

3.5 Accretion features

The mass inflow is usually traced by the inversed P Cyg (IPC) profiles of some diagnostic lines. In the optical region these are the higher Balmer lines, the He I lines and the triplet O I 7773 Å. These indicators are strong in actively accreting cTTS, but absent in spectra of FUors. In V1331 Cyg, the IPC profiles are not well expressed, although noticeable in the He I 5876 Å, where the red wing of the emission is depressed by the red-shifted absorption (Fig. 6, left panel). A slight asymmetry can be noticed also in the less blended Paschen 14 line.

Another indication is the broad absorption blend of the triplet O I 7773 Å (Fig. 6, right panel). This feature is present in the spectra of 1998 and 2012, but falls out of spectral order in the Keck spectra of 2004 and 2007. In both spectra of 1998 and 2012, the red wing of the absorption is extended to about $+200$ km s⁻¹, which is in agreement with the He I profile. We may conclude that mass infall is going on in V1331 Cyg and the projected infall velocity is about 200 km s⁻¹.

The apparent weakness of signatures of mass accretion in V1331 Cyg is probably related to the pole-on orientation of the star. Besides of the mass accretion rate and the viewing angle, the strength of the red-shifted absorption depends

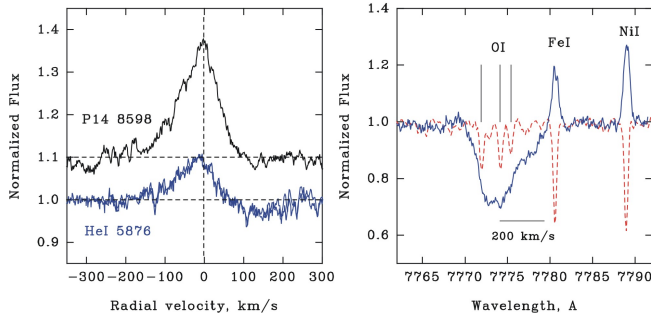


Figure 6. Signatures of accretion in V1331 Cyg. Left panel: line profiles of He I 5876 Å and Pashen 14, shifted by 0.1 for clarity. Right panel: triplet of O I (7772, 7774 and 7775 Å) in β Aqr (dashed line) and V1331 Cyg (solid line). In V1331 Cyg, the red wing of the blend is extended to about 200 km s^{-1} .

also on the size of magnetosphere and the gas temperature (Muzerolle et al. 2001).

3.6 ‘Shell’ features

One peculiarity of V1331 Cyg spectrum is the presence of blue-shifted absorption components of the emission lines of metals. These are so-called ‘shell’ lines – a signature of expanding gaseous shells. In our spectra of V1331 Cyg the ‘shell’ components are present in the following lines: Fe II 4924 and 5118 Å, Mg I 5183 Å, Li I 6707 Å, K I 7699 Å, and Na I D (see Figs 1 and 7). In the resonance line K I 7699 Å, there is one distinct narrow ‘shell’ feature at -240 km s^{-1} . The same is present in the resonance Na I doublet, although saturated and blended with the wider P Cyg absorption. In the Fe II and Mg I, the ‘shell’ profile is more complicated, although the component at -240 km s^{-1} is present there too. The component at -240 km s^{-1} is stable over the years of our observations, while the overall profile varies from year to year. No variability in the ‘shell’ lines was found in the 20-d period of our monitoring in 2012. We may conclude that the ‘shell’ components vary on a time-scale of a year. With the velocity of 240 km s^{-1} , this time of variability corresponds to the distance scale of about 50 au.

There is a striking similarity in velocity profiles of the ‘shell’ lines and the forbidden lines (Fig. 8). The Mg I and [O I] profiles look like a mirror reflection of each other. We know that the blue-shifted component of the forbidden emission lines is formed in jets of TTS (e.g. Hartigan et al. 1995) at large distance (tens of au) from the star, where ionized atoms recombine in the cooling region behind the shock. The similarity of the ‘shell’ profiles with those of the forbidden lines strongly suggests that the ‘shell’ absorptions also arise in the post-shocked gas in the jet. With low inclination, we see the star through the jet, and the line of sight (LOS) to the star intersects all the shocks in the jet. The gas density is low, but the length scale is long enough to get the column density of atoms necessary to form the ‘shell’ absorption.

4 ANALYSIS: WIND MODEL

The stellar luminosity and temperature of V1331 Cyg place the star on the beginning of the radiative track for mass

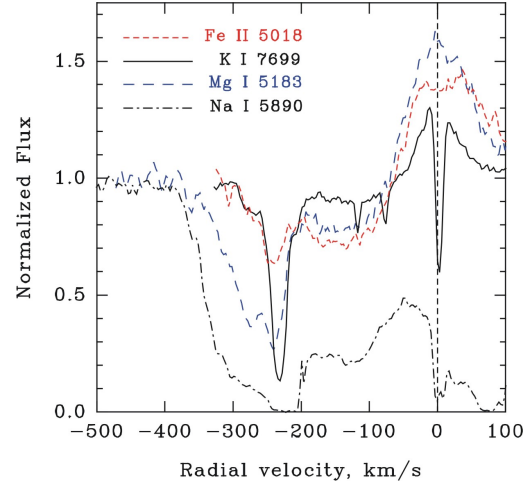


Figure 7. The blueshifted ‘shell’ lines of Mg I, Fe II, K I and Na I with maximum absorption at about -240 km s^{-1} . The spectrum of 1998.

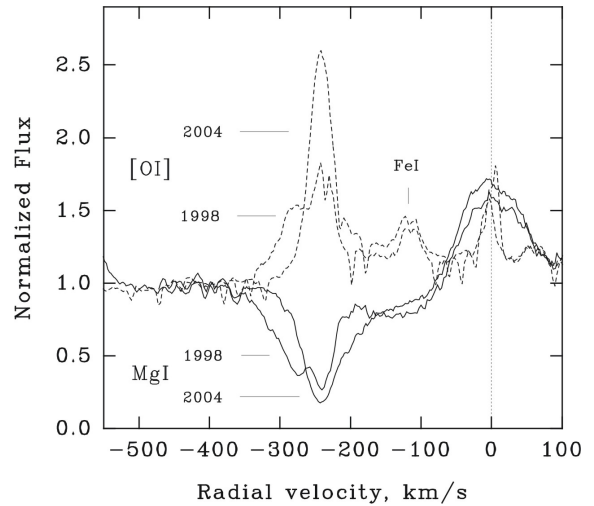


Figure 8. Comparison of the forbidden [O I] 6300 Å emission profile (dashed curves) and the blue-shifted ‘shell’ absorption of Mg I 5183 Å (solid line) in 1998 and 2004. The weaker emission peak at -120 km s^{-1} belongs to Fe I 6297.8 Å.

$2.8 M_{\odot}$, in between TTS and Herbig Ae stars, at the age of about 1.5 Myr. Since the star is oriented near pole-on to observer, it is hard to expect any effect of rotational modulations. The irregular light variability is probably caused by only the accretion processes. Thus, the period of rotation remains unknown. Further, the small inclination angle of V1331 Cyg implies that the LOS to the star (the continuum radiation source) cannot intersect a disc wind. Consequently, the wide and deep blueshifted wind absorption feature seen in $H\alpha$ and $H\beta$ (Figs 4 and 5) are not possible with this wind configuration. Most likely, such absorption features are caused by a stellar wind that arises in the polar directions (e.g. Edwards et al. 2006; Kwan, Edwards & Fischer 2007; Kurosawa et al. 2011). For an observer located in the polar direction, not only the LOS to the stellar surface can easily pass through the stellar wind, but also it can intersect with a full range of velocity surfaces which provide

Table 2. Adopted model parameters

R_* (R_\odot)	M_* (M_\odot)	T_{eff} (K)	R_{mi} (R_*)	R_{mo} (R_*)	T_{m} (K)	\dot{M}_a ($\dot{M}_\odot \text{yr}^{-1}$)	T_w (K)	v_∞ (km s^{-1})	v_0 (km s^{-1})	β ...	R_0 (R_*)
5.0	2.8	5200	3.0	3.8	5500	2×10^{-6}	9000	530	10	1.8	3.8

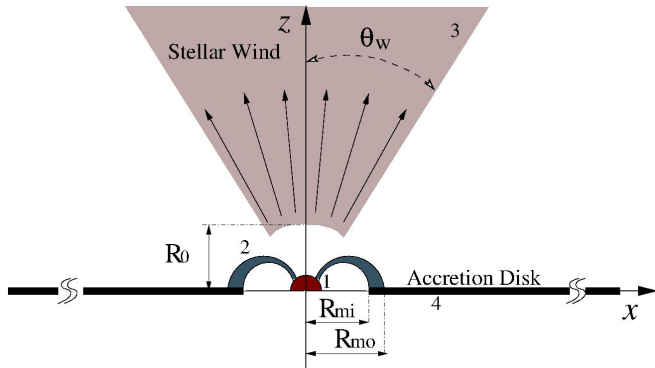


Figure 9. Basic model configuration of the stellar wind-magnetosphere hybrid model. The model is axisymmetric and it consists of four components: (1) the continuum source (star) located at the origin of the Cartesian coordinates system (x, z) , (2) the magnetospheric accretion flow, (3) the (bipolar) stellar wind, and (4) the optically thick but geometrically thin accretion disc. The wind is launched from a sphere with radius R_0 , but is restricted within the cones with the half opening angle θ_w . The density distribution is symmetric around the z -axis. The figure is not to scale.

a possibility to form the wide and deep blueshifted absorption feature in the Balmer lines. For this reason, we mainly focus on modelling the observed line profiles using the bipolar stellar wind and on probing its overall characteristics. In the following, we briefly describe our line profile models, and present the comparison of our models with observed $H\alpha$ and $H\beta$ line profiles.

4.1 Model configuration

To model emission line profiles of $H\alpha$ and $H\beta$, we use the radiative transfer code TORUS (e.g. Harries 2000; Kurosawa et al. 2006, 2011). In particular, the numerical method used in the current work is essentially identical to that in Kurosawa et al. (2011). The model uses the adaptive mesh refinement grid in Cartesian coordinate and assumes an axisymmetry around the stellar rotation axis. The model includes 20 energy levels of hydrogen atom, and the non-local thermodynamic equilibrium (non-LTE) level populations are computed using the Sobolev approximation (Sobolev 1957; Castor 1970). For more comprehensive descriptions of the code, readers are referred to Kurosawa et al. (2011).

A basic schematic diagram of our model is shown in Fig. 9. The model includes two flow components: (1) the dipolar magnetospheric accretion as described by Hartmann, Hewett & Calvet (1994) and Muzerolle, Calvet & Hartmann (2001), and (2) the stellar wind emerging from the polar regions. The radiation from hotspots/rings formed on the stellar surface is also included. An optically thick and

Table 3. Model Parameters for Line Fits

Model ID ...	\dot{M}_w ($\dot{M}_\odot \text{yr}^{-1}$)	θ_w ...
A	6.0×10^{-8}	50°
B	9.0×10^{-8}	50°
C	1.1×10^{-7}	50°
D	9.0×10^{-8}	40°
E	9.0×10^{-8}	60°

geometrically thin disc is placed on the equatorial plane to imitate the absorption by the accretion disc.

The accretion stream through a dipolar magnetic field is described as $r = R_m \sin^2 \theta$ (e.g. Ghosh, Pethick & Lamb 1997; Hartmann et al. 1994) where r and θ are the polar coordinates; R_m is the magnetospheric radius at the equatorial plane. The accretion funnel regions are defined by two stream lines corresponding to the inner and outer magnetospheric radii, i.e., $R_m = R_{\text{mi}}$ and R_{mo} . We adopt the density and temperature structures along the stream lines as in Hartmann et al. (1994). The temperature scale is normalized with a parameter T_m which sets the maximum temperature in the stream.

The stellar wind is approximated as outflows in narrow cones with their half-opening angle θ_w . Here, we assume the flow is only in the radial direction, and its velocity is described by the classical beta-velocity law (cf. Castor & Lamers 1979):

$$v_r(r) = v_0 + (v_\infty - v_0) \left(1 - \frac{R_0}{r}\right)^\beta, \quad (1)$$

where v_∞ and v_0 are the terminal velocity and the velocity of the wind at the base ($r = R_0$). Assuming the mass-loss rate by the wind is \dot{M}_w and using the mass-flux conservation in the flows, the density ρ_w of the wind can be written as:

$$\rho_w(r) = \frac{\dot{M}_w}{4\pi r^2 v_r(r) (1 - \cos \theta_w)}. \quad (2)$$

Note that ρ_w becomes that of a spherical wind when $\theta_w = 90^\circ$. The temperature of the stellar wind (T_w) is assumed isothermal as in Kurosawa et al. (2011). To avoid an overlapping of the stellar wind with the accretion funnels, the base of the stellar wind (R_0) is set approximately at the outer radius of the magnetosphere (R_{mo}) (cf. Fig. 9).

4.2 Balmer line models

The basic stellar parameters adopted for modelling the observed $H\alpha$ and $H\beta$ profiles of V1331 Cyg are: $M_* = 2.8 M_\odot$, $R_* = 5 R_\odot$ and $T_{\text{eff}} = 5200$ K, as found in Section 3.1. Since we do not find a clear periodic signature in the 20-d spectroscopic monitoring of V1331 Cyg (Sect. 3.4), we roughly esti-

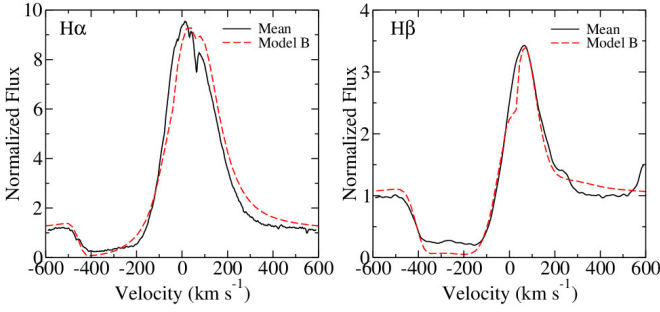


Figure 10. Comparisons of the mean H α and H β profiles from the 2012 observations (solid; cf. Table 1) with Model B (dashed; Table 3). The matches between the model and the observations are excellent. The very wide and deep blueshifted absorption component (the P-Cyg line profile feature) is well produced with the bipolar outflow (the stellar wind) in our model.

mate the period by using $v \sin i < 6 \text{ km s}^{-1}$ and $R_* = 5.0 R_\odot$ (Sect. 3.1). We assume a low inclination angle $i = 10^\circ$, which sets lower limits to the period of stellar rotation $P_* \geq 7.4$ d and the corotation radius $R_{\text{cr}} \geq 4.5 R_*$. The inner and outer magnetospheric radii are set to $R_{\text{mi}} = 3.0 R_*$ and $R_{\text{mo}} = 3.8 R_*$, which are slightly smaller than the corotation radius. Other important model parameters adopted are summarized in Table 2. Note that P_* and i used here are rough estimates, and are only needed to find a reasonable size of the magnetosphere.

To model the line variability behaviours seen in the observations (Figs. 4 and 5), we mainly concentrate on the effect of varying the wind mass-loss rate (\dot{M}_w) and the half-opening angle of the bipolar stellar wind (θ_w) as in Table 3. To find a reasonable base model for the line variability, we first fit the mean H α and H β profiles from the 20-d spectroscopic monitoring in 2012 (cf. Table 1). The results of the model fits are shown in Fig. 10. The model uses $\dot{M}_w = 9.0 \times 10^{-8} M_\odot \text{ yr}^{-1}$ and $\theta_w = 50^\circ$ (Model B in Table 3). Overall agreement of the model and the observed mean profiles is very good. The model reproduces the deep and wide absorption of the P-Cyg profiles very well. The line strengths and the widths are matched well with the observations also. However, the wind absorption depth of H β tends to be slightly stronger in the model. In this model, the emission component in both lines is mainly originated in the wind. The contribution of the magnetosphere to the line emission is much smaller, but it is important for producing a slightly wider emission component than that from the wind emission alone. This model (Model B) is used as our base for the line variability modelling which will be presented next. This model also sets the common model parameter values given in Table 2.

Next, we examine the line variability that occurs in the time-scale of about one week. For this purpose, we focus on the H α and H β profiles observed at approximately 8 d apart, namely the data from 2012 Aug. 14 and Aug. 22 (the third and the last entries of Calar Alto observations in Table 1). The corresponding line profiles are shown in the top panels of Fig. 11. The figure shows that the peak intensity of H α increases by a factor of 1.25, and that of H β increases by a factor of 1.1 during 8 d. The maximum extent of wind absorption does not change significantly during this time. In general, the line shapes do not change dramatically in

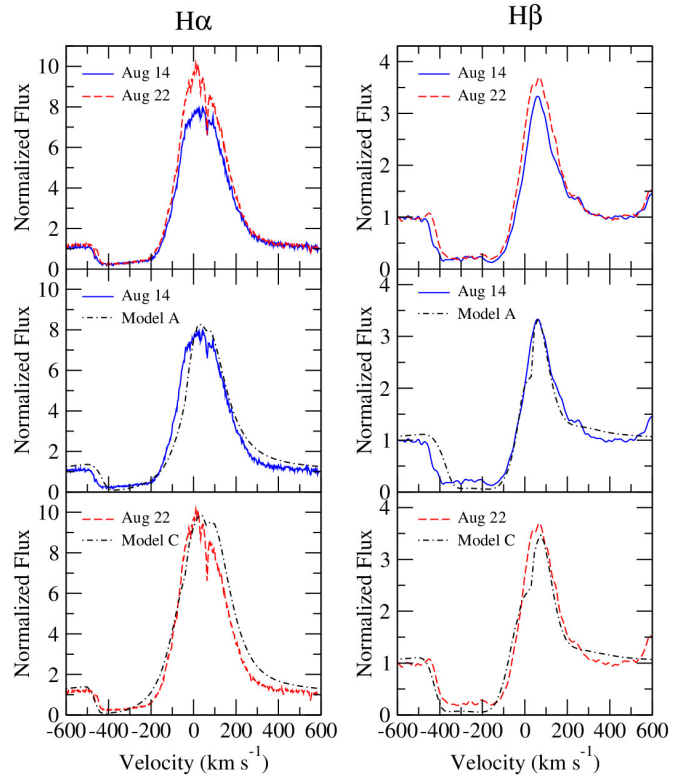


Figure 11. Top panels: the variability of H α and H β in about 8 d time-scale, i.e. between Aug. 14 (solid) and Aug. 22 (dashed) in 2012. Middle panels: the model line profiles (Model A in Table 3) that fit the observation from 2012 Aug. 14. Bottom panels: the model line profiles (Model C in Table 3) that fit the observation from 2012 Aug. 22. The ranges of line variability seen in the observations at this time-scale are well reproduced by changing the mass-loss rate in the bipolar stellar wind from $6.0 \times 10^{-8} M_\odot \text{ yr}^{-1}$ (Model A) to $11 \times 10^{-8} M_\odot \text{ yr}^{-1}$ (Model C).

this time-scale (see also Fig. 5), indicating the overall flow structures of V1331 Cyg is stable in the time-scale of one week.

The relatively small variability seen in the observations is well reproduced by our models (Models A and B in the middle and lower panels of Fig. 11) by changing the wind mass-loss rate (\dot{M}_w) slightly from our base model (Model B). The range of the mass-loss rates that fit the observed variability in 8 d period is $(6\text{--}11) \times 10^{-8} M_\odot \text{ yr}^{-1}$. This relatively small change in the mass-loss rate is perhaps caused by the response or adjustment of the outflow to a change in the mass-accretion rate. The fluctuation in the mass-accretion rate by a factor of ~ 2 naturally occurs and is often observed in the MHD simulations of accretions on to cTTS through a magnetosphere (e.g. Romanova et al. 2002). Although we kept the mass-accretion rate in Models A and C at a constant value (Table 2), the effect of changing the mass-accretion on H α and H β line profiles is much smaller than that of changing the wind mass-loss rates because the wind emission dominates the observed line profiles, as we found earlier.

As briefly mentioned earlier in Section 3.4, the variability of H β in the time-scale of years (Fig. 4; also in the left panel in Fig. 12) is also not so very large. As shown in Fig. 12, the peak intensity remains almost constant except

for the data from 2007 which is about 10 per cent higher than those of other years. A more notable variability is seen in the maximum velocity (v_{\max}) of the blueshifted absorption component in the observed H β profiles. From Fig. 12, we find v_{\max} changes approximately between -350 and -450 km s $^{-1}$.

This type of variability is well reproduced by adjusting the half-opening angle (θ_w) of the bipolar wind between 40° and 60° (Models B, D and E in Table 3), while keeping all other parameters fixed. The corresponding line profiles are shown and compared with the observations in Fig. 12. The models show a similar range of v_{\max} values as in the observations. Interestingly, in these models, the terminal velocity of the wind (v_∞ in equation 1) is fixed at the constant value of 530 km s $^{-1}$ which is higher than the v_{\max} values. Here, the change in the value of v_{\max} in the models can be understood by the change in the optical depth of the wind. Because the wind mass-loss rate is fixed in these models, the density of the wind increases as the half-opening angle (θ_w) of the wind decreases (see equation 2). Hence, the high optical depth region in the wind, which causes the blueshifted absorption, extends to a larger radius for a smaller θ_w . This results in a larger value of v_{\max} or the *apparent* terminal velocity. Note that the value v_{\max} can be smaller than v_∞ when the optical depth is significantly below 1 at outer radii where the wind speed reaches $\sim v_\infty$.

Since very little is known about the formation process of the stellar wind in cTTS itself, the physical cause of the change in the wind opening angle is also unknown. Here, we speculate that the change in θ_w may be caused by (1) the change in the strengths of the open magnetic field in the polar direction, and/or (2) the change in the collimation of an external wind such as the conical wind (Romanova et al. 2009) which can influence the flow geometry of the stellar wind. See Section 5 for a further discussion on this issue.

In summary, our model with the bipolar stellar wind agrees well with the general characteristics of the observed H α and H β profiles from V1331 Cyg. Rather small variabilities seen in a week to several-year time-scales can be reasonably reproduced by changing the mass-loss rate and the opening angle of the stellar wind.

5 DISCUSSION

Our studies show that a strong stellar wind is required to explain the P Cyg features in Balmer lines of V1331 Cyg. The comparisons of our models with the observations show that this stellar wind is a necessary component of the flow. It is not clear however, whether this wind can solely explain the outflows observed at much larger distances from the star. It may be possible that some other mechanisms of outflow also contribute to the matter flux, such as the disc wind (e.g. Zanni et al. 2007) and conical wind from the disc-magnetosphere boundary (e.g. Romanova et al. 2009). The matter flux in the stellar wind used in our models is about (3–5.5) per cent of the matter flux in the disc (see Tables 2 and 3), which is within the range of those found in observations, $\sim(0.1\text{--}10)$ per cent (e.g. Hartigan et al. 1995; Edwards et al. 2006; Calvet 1998); therefore, the matter flux used in our model could be sufficient to explain the large-scale outflows. However, the opening angle of the stellar wind

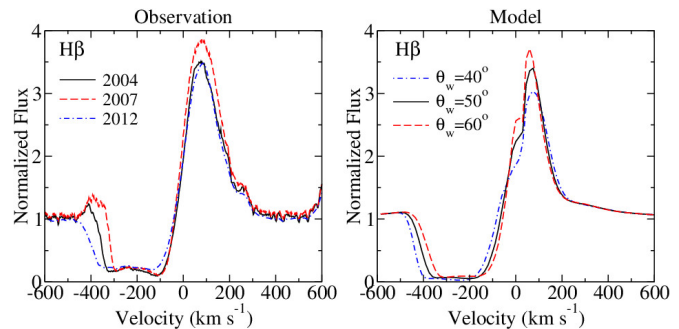


Figure 12. A comparison of the variability observed in H β in the time-scale of several years (*left panel*) with our radiative transfer models (*right panel*). The variability in H β seen in this time-scale can be roughly reproduced by changing the half-opening angle (θ_w) of the bipolar stellar wind in our model between 40° and 60° , i.e., Models D and E in Table 3, respectively. The models show similar ranges of variability in the peak line flux and the extent (apparent maximum velocity) of the blueshifted wind absorption component as in the observations. N.B. the observed H β shown in the left panel are same as those in Fig. 4, but we omitted the data from 1998 for clarity.

adopted in our model is relatively large ($\theta_w = 40^\circ - 60^\circ$), hence this wind should be somehow collimated at larger distances, because the high-velocity jet component is usually well collimated. Alternatively, it is possible that both stellar and inner disc winds contribute to the outflow. Usually, the disc wind and conical wind have also a large opening angle in the beginning of the flow, and hence they will not restrict the wide-angle stellar wind, which is needed for explaining the Balmer lines. However, these inner disc winds may influence the collimation of the stellar wind.

In this study, we suggest that the variability seen in the Balmer lines may be connected with changes of the opening angle θ_w due to inner disc winds (see Section 4.2). For example, in case of conical winds, the degree of collimation varies depending on the level of magnetization σ (ratio of the magnetic to matter pressure) in the outflow. In case of low magnetization, $\sigma < 0.01$ the conical winds are only weakly collimated inside the simulation region (Romanova et al. 2009), while in cases of higher magnetizations, $\sigma \sim (0.1 - 0.3)$, the collimation is much stronger (Königl, Romanova & Lovelace 2011; Lii, Romanova & Lovelace 2012). Therefore, a small variation in the magnetic flux threading conical winds may lead to a variation in the collimation of stellar winds and consequently a variation of the shape of Balmer lines.

Recent MHD models of stellar winds from cTTS (e.g. Matt & Pudritz 2005, 2008; Cranmer 2009) suggest that the wind is ‘accretion-powered.’ Their studies indicate that the mass-loss and mass-accretion rates are coupled, i.e., the mass-loss rate would increase if the accretion-rate increases. On the other hand, the MHD simulations by Romanova et al. (2009) and Lii et al. (2012) have shown that the opening angle of the external wind (the conical wind) decreases when the mass-accretion rate increases.

Combining the results from these studies, we expect the wind mass-loss rate would become larger if the opening angle of the stellar wind becomes smaller. In our simple wind model (equations 1 and 2), if the mass-loss rate increases and the opening angle decreases, the density of the wind would

increase, assuming the velocity structure of the wind does not change. In general, if the mass-accretion rate increases, the energy available to drive the wind would also increase; hence, a stronger wind is expected to arise, i.e., with a higher mass-loss rate and a higher terminal velocity.

In our line profile models (Section 4.2), we found a change in the mass-loss rate can explain the variability on small time-scales (days/weeks), but on larger time-scales (several years), a change in the opening angle would play a more important role. As we have mentioned above, in reality a change in mass-accretion rate and a change in opening angle might be coupled. This may indicate that the changes in mass-accretion rates on shorter time-scales (days/weeks) are much smaller (hence no/little change in the opening angle) than those on longer time-scales (several years). Since a change in the opening angle of the wind could be also caused by a change in the strength of the stellar magnetic field, our line profile analysis may suggest that the magnetic field strength is relatively stable on small time-scales (days/weeks), but it changes significantly in longer time-scales (several years).

The high mass-accretion rate, $\dot{M}_a = 2 \times 10^{-6} M_\odot \text{ yr}^{-1}$, adopted in our model (Section 4.2), places the star near the top end of the full range of accretion rates observed in cTTS (e.g. Hartigan et al. 1995; Edwards et al. 2006).

After finding the best fit model to the observed mean line profiles of $H\alpha$ and $H\beta$ (Fig. 10), we examined the sensitivity of the model to a change in mass-accretion rate. This was done to check the acceptable range of mass-accretion rates with which the model can reasonably fit the observed $H\alpha$ and $H\beta$ shown in Fig. 10. We find such range to be $\dot{M}_a = (1.5\text{--}2.5) \times 10^{-6} M_\odot \text{ yr}^{-1}$.

On the other hand, a slightly lower accretion rate follows from the observed fluxes in $H\alpha$ and $\text{He I } 5876 \text{ \AA}$ emissions. Using the empirical relationships between the line luminosities and mass accretion rates found in Rigliaco et al. (2012) (see also Mohanty, Jayawardhana & Basri 2005; Herczeg & Hillenbrand 2008; Fang et al. 2009), we find the mass-accretion rate of V1331 Cyg to be $\dot{M}_a = 0.7^{(+1.5)}_{(-0.5)} \times 10^{-6} M_\odot \text{ yr}^{-1}$. Note that the effect of veiling is not included in this estimate. In Section 3.2, we found that the VF between 4500 and 8500 \AA is rather uncertain, but the upper limit is $\text{VF} \leq 1$. This means \dot{M}_a estimated from the line luminosities could be higher by a factor of up to 2. Considering the uncertainties, the mass-accretion rate used in our model reasonably agrees with the value estimated from the line luminosity measurements.

The emission line spectrum of V1331 Cyg resembles that of the jet-driving Class I type young object V2492 Cyg (Hillenbrand et al. 2012). In both objects, besides the Balmer and other wind-sensitive lines, indicating intensive mass outflow, there are many permitted emission lines of low excitation, neutral and singly ionized metals, which are relatively narrow ($\approx 50 \text{ km s}^{-1}$) and rested at stellar velocity. Interestingly, a weak $\text{Li I } 6707 \text{ \AA}$ emission was noticed in V2492 Cyg. It is also present in V1331 Cyg, being superposed with narrow photospheric absorption of the same transition. The appearance of $\text{Li I } 6707 \text{ \AA}$ in emission at stellar velocity was noticed earlier in spectra of the FUor V1057 Cyg (Herbig 2009). Apparently, in V1331 Cyg, there must be a volume of low-temperature, low-density gas which is not involved in the accretion/wind motions.

As shown in Section 3.6, the striking similarity in velocity profiles of the ‘shell’ absorptions of metals and the forbidden emissions of $[\text{O I}]$ strongly suggests the origin of the ‘shell’ absorptions in the post-shocked gas in the jet, i.e. the jet is projected to the star. This might imply rather a small inclination angle, provided the jet is straight and normal to the disc plane. However, in the $[\text{S II}]$ image of V1331 Cyg vicinity, a wiggling jet was traced to as far as 360 arc-sec (Mundt & Eisloffel 1998), i.e. the jet is deviated of a straight line at large distances from the star. In our wind model we assume inclination $i = 10^\circ$, but the resulted line profiles remain about the same even if the inclination is decreased by factor of 2.

The ‘shell’ absorptions are not typical for cTTS but is common for the classical FUors V1057 Cyg and FU Ori (Mundt 1984; Herbig et al. 2003; Herbig 2009). The two FUors inclined differently, so that a jet (if any) does not point to observer, but the wind is much stronger than in V1331 Cyg. Probably the ‘shell’ lines in FUors are formed not in distinct expanding shells, but in the shocks within their powerful extended wind flows. The case of V1331 Cyg is rare in a sense that the star is seen through its jet, so it may be considered as a *stellar analogue of blazar*.

6 CONCLUSIONS

From the analysis of the high-resolution spectra of the pre-FUor V1331 Cyg we conclude the following:

- the highly veiled photospheric spectrum belongs to G7-K0 IV star of mass $2.8 M_\odot$ and radius $5 R_\odot$. The intrinsic width of the photospheric lines is not resolved, $v \sin i < 6 \text{ km s}^{-1}$, i.e. the star is seen pole-on.
- the amount of veiling depends on line strength. The effect may be caused by abnormal structure of atmosphere heated by mass accretion.
- the blue-shifted absorption of Fe II , Mg I , K I and some other metals form in a post-shocked gas within a jet.
- the Balmer line profiles are reproduced by model of bipolar stellar wind with mass-loss rate $(6\text{--}11) \times 10^{-8} M_\odot \text{ yr}^{-1}$.
- the Balmer line profile variabilities in several days to years time-scales are reproduced by changes in mass-loss rate and opening angle of the stellar wind, which may be caused by small variations of magnetic flux threading the inner wind.
- in addition to the stellar wind, responsible for the observed P Cyg line profiles, the presence of conical wind and/or disc wind is suggested to explain the collimation at large distances.

In this work we considered only one specific case of a pre-FUor wind blowing towards the observer, where the stellar wind component is dominant in formation of the observed line profiles. It would be interesting to do similar study of wind(s) in a pre-FUor viewed at different inclination, e.g. LkHa 321, so that the disc wind (or conical wind) properties could also be investigated.

ACKNOWLEDGEMENTS

We thank the referee, Thomas Haworth, for valuable comments which helped us improve the clarity of the manuscript. Major parts of this work is based on the Keck spectra of V1331 Cyg kindly provided to one of us (PP) by George Herbig in 2009. We are grateful to Antonio Pedrosa for the spectrum taken in 1998. MF acknowledges financial support from grants AYA2011-30147-C03-01 of the Spanish Ministry of Economy and Competitivity (MINECO), co-funded with EU FEDER funds, and 2011 FQM 7363 of the Consejería de Economía, Innovación, Ciencia y Empleo (Junta de Andalucía, Spain). Research of MMR was supported by NASA grant NNX11AF33G and NSF grant AST-1211318. RK thanks Suzan Edwards, Greg Herczeg and Stanislav Melnikov for valuable discussions.

REFERENCES

- Aceituno J. et al. 2013, *A&A*, 552, 31
 Audard M. et al. 2014, preprint (arXiv1401.3368A)
 Batalha C.C., Stout-Batlha N.M., Basri G., Terra M.A.O. 1996, *ApJS*, 103, 211
 Beristain G., Edwards S., Kwan J. 1998, *ApJ*, 499, 828
 Bouvier J., Alencar S.H.P., Harries T.J., Johns-Krull C.M., Romanova M.M., 2007, in Reipurth B., Jewitt D., Keil K., eds, *Protostars and Planets V*. University of Arizona Press, Tucson, p. 479
 Berdyugina S.V. 1991, *Bull. Crimean Astrophys. Obs.*, 83, 89
 Calvet N., 1988, *AIP Conf. Proc. Vol. 431, Accretion Processes in Astrophysical Systems: Some Like it Hot! – Eight Astrophysics Conference*. Am. Inst. Phys., New York, p. 495
 Castor J. I. 1970, *MNRAS*, 149, 111
 Castor J. I., Lamers H. J. G. L. M. 1979, *ApJS*, 39, 481
 Chavarría C. 1981, *A&A*, 101, 105
 Cohen M., Kuhl L. V. 1979, *ApJSS*, 41, 743
 Cranmer S. R. 2009, *ApJ*, 706, 824
 Dodin A.V., Lamzin S.A. 2012, *Astron. Lett.*, 38, 649
 Edwards S., Fischer W., Hillenbrand L., Kwan J. 2006, *ApJ*, 646, 319
 Eisner J. A., Hillenbrand L. A., White R. J., Bloom J. S., Akeson R. L., Blake C. H. 2007, *ApJ*, 669, 1072
 Fang M., van Boekel R., Wang W., Carmona A., Sicilia-Aguilar A., Henning Th. 2009, *ApJ*, 504, 461
 Fernandez M., Eiroa C. 1996, *A&A*, 310, 143
 Gahm G. F., Walter F. M., Stempels H. C., Petrov P. P., Herczeg G. J. 2008, *A&A*, 482, L35
 Gahm G. F., Stempels H. C., Walter F. M., Petrov P. P., Herczeg G. J. 2013 *A&A*, 560, 57
 Ghosh P., Pethick C. J., Lamb, F. K. 1977, *ApJ*, 217, 578
 Goodrich R.W. 1987, *PASP*, 99, 116
 Guenther H.M. 2013, *Astron. Nachr.*, 334, 1
 Hamann F., Persson S. E. 1992, *ApJS*, 82, 247
 Harries T. J. 2000, *MNRAS*, 315, 722
 Hartigan P., Edwards S., Ghandour L. 1995, *ApJ*, 452, 736
 Hartmann L., Hewett R., Calvet N. 1994, *ApJ*, 426, 669
 Hartmann L., Kenyon S. J. 1996, *ARA&A*, 34, 207
 Herbig G. H. 1989, *ESO Workshop on Low Mass Star Formation and Pre-Main Sequence Objects*, p. 233
 Herbig G. H. 1990, *ApJ*, 360, 639
 Herbig G. H., Petrov P.P., Duemmler R. 2003, *ApJ*, 595, 384
 Herbig G. H. 2009, *AJ*, 138, 448
 Herczeg G. J., Hillenbrand L. A. 2008, *ApJ*, 681, 594
 Hillenbrand L. A. et al., 2013, *AJ*, 145, 59
 Kolotilov E.A. 1983, *Sov. Astron. Lett.*, 9, 289.
 Königl A., Romanova M.M., Lovelace R. V. E. 2011, *MNRAS*, 416, 757
 Kuhl L. V. 1964, *ApJ*, 140, 1409
 Kupka F., Ryabchikova T. A., Piskunov N. E., Stempels H. C., Weiss, W. W. 2000, *Balt. Astron.*, 9, 590
 Kurosawa R., Harries T. J., Symington N. H. 2006, *MNRAS*, 370, 580
 Kurosawa R., Romanova M. M., Harries T. J. 2011, *MNRAS*, 416, 2623
 Kwan J., Edwards S., Fischer, W. 2007, *ApJ*, 657, 897
 Kwan J., Fischer W. 2011, *MNRAS*, 411, 2383
 Lii P., Romanova M.M., Lovelace R.V.E. 2012, *MNRAS*, 420, 2020
 McMuldrough S., Sargent A.I., Blake, G.A. 1993, *AJ*, 106, 2477
 Matt S., Pudritz R.E. 2005, *ApJ* 632 L135
 Matt S., Pudritz R.E. 2008, *ApJ*, 678, 1109
 Mohanty S., Jayawardhana R., Basri G. 2005, *ApJ*, 626, 498
 Mundt R., Appenzeller I., Bertout C., Krautter J., Chavarría C. 1981, *A&A*, 93, 412
 Mundt R. 1984, *ApJ*, 280, 749
 Mundt R., Eisloffel J. 1998, *AJ* 116, 860
 Muzerolle J., Calvet N., Hartmann L. 2001, *ApJ*, 550, 944
 Petrov P. P., Gahm G. F., Stempels H. C., Walter F. M., Artemenko, S. A. 2011, *A&A*, 535, A6
 Petrov P. P., Babina E. V. 2014, *Bull. Crimean Astrophys. Obs.*, 110, 1
 Pudritz R. E., Ouyed R., Fendt Ch., Brandenburg A., 2007, in Reipurth B., Jewitt D., Keil K., eds, *Protostars and Planets V*. University of Arizona Press, Tucson, p. 277
 Quanz S. P., Apai D., Henning Th. 2007, *ApJ*, 656, 287
 Romanova M. M., Ustyugova G. V., Koldoba A. V., Lovelace R. V. E. 2002, *ApJ*, 578, 420
 Romanova M. M., Ustyugova G. V., Koldoba A. V., Lovelace R. V. E. 2009, *MNRAS*, 399, 1802
 Rigliaco E., Natta A., Testi L., Randich S., Alcalá J. M., Covino E., Stelzer B., 2012, *A&A*, 548, 56
 Shevchenko V. S., Grankin K. N., Ibragimov M. A., Mel'nikov S. Yu., Yakubov, S. D. 2003, *Ap&SS*, 202, 121
 Shu F.H., Najita J., Ostriker E., Wilkin F., Ruden S., Lizano S., 1994, *ApJ*, 429, 781
 Siess L., Dufour E., Forestini M. 2000, *A&A*, 358, 593
 Sobolev V. V. 1957, *Soviet Astron.*, 1, 678
 Valenti J.A., Basri G., Johns, C.M. 1993, *AJ*, 106, 2024
 Welin G. 1976, *A&A*, 49, 145
 Zanni C., Ferrari A., Rosner R., Bodo G., Massaglia S. 2007, *A&A*, 469, 811